Available online at www.sciencedirect.com
SCIENCE DIRECT®

Journal of the European Ceramic Society 23 (2003) 1391–1400
www.elsevier.com/locate/jeurceramsoc

# Characterization of $CaTiO_3$-$NdAlO_3$ dielectric ceramics

Bostjan Jancar*, Danilo Suvorov, Matjaz Valant, Goran Drazic

*"Jozef Stefan" Institute, Ljubljana, Slovenia*

Received 22 March 2002; received in revised form 10 September 2002; accepted 16 September 2002

**Abstract**

An X-ray analysis of the $(1-x)CaTiO_3$–$xNdAlO_3$ tie line revealed solid solubility across the entire compositional range. For $x<0.85$ the crystal structure of the solid solution is that of the orthorhombically distorted perovskite, which is also the structure of pure $CaTiO_3$, whereas solid solutions with $x>0.90$ exhibit the trigonal structure, characteristic of pure $NdAlO_3$. With the increase in $x$ the permittivity, the temperature coefficient of resonant frequency and the dielectric losses decrease. Ceramics based on the $0.7CaTiO_3$–$0.3NdAlO_3$ solid solution exhibit $\tau_f \approx 0$ ppm/K, $\varepsilon_r = 44$ and a $Q$-value that varies between 30000 and 45000 GHz depending on the cooling rate after the sintering. A microstructural analysis revealed the presence of twin related domains, antiphase boundaries and two types of inclusions rich in Al: hexagonal $CaAl_{12}O_{19}$-based inclusions and the spinel $MgAl_2O_4$, which results from the Mg-based impurities.


*Keywords:* $CaTiO_3$; Defects; Dielectric properties; Inclusions; Microstructure; $NdAlO_3$

## 1. Introduction

Due to their high relative permittivities, the alkaline-earth titanates with their perovskite structure have been of great interest to the electronics industry over the past 30 years. Most of the research was focused on ferroelectric $BaTiO_3$-based ceramics, which have been extensively utilized in the production of low-frequency electronic devices. In the last decade, however, the expansion of microwave technologies has resulted in the need for a new generation of dielectric materials. For applications in the microwave frequency region research has focused on paraelectric rather than ferroelectric materials. The main objective has been the development of a dielectric material with a high relative permittivity ($\varepsilon_r$), low dielectric losses (high $Q$-values) and a tunable temperature coefficient of resonant frequency ($\tau_f$).

Some of the first data on the dielectric properties of $CaTiO_3$ was published by Kell et al. in the early 1970s.[1] They reported that $CaTiO_3$ exhibits a combination of high permittivity ($\varepsilon_r = 170$) and modest dielectric losses ($Q \times f = 3500$ GHz), which makes it a suitable candidate for microwave applications. The major disadvantage of $CaTiO_3$ is its high temperature dependence of permittivity: the reported value for its temperature coefficient of pemittivity is $\tau_{\varepsilon} = -1850$ ppm/K (or in terms of temperature coefficient of resonant frequency $\tau_f \approx +800$ ppm/K).[1] As a result the first objective when synthesizing any new $CaTiO_3$-based microwave material is to suppress the large positive $\tau_f$.

Over the last 10 years a variety of research work describing $CaTiO_3$-based materials and their microwave dielectric properties has been published.[2–7] Kim et al.[4] reported that the partial substitution of $Ca^{2+}$ with $La^{3+}$ leads to the formation of single-phase $Ca_{1-x}La_{2x/3}TiO_3$ solid solutions with the structure changing from orthorhombic to tetragonal double-layered perovskite as $x$ increases. A decrease in $\varepsilon_r$, $\tau_f$ and the dielectric losses with an increase in $x$ were reported, however, complete suppression of the positive $\tau_f$ was not achieved. Similar results were obtained for the $Ca_{1-x}Nd_{2x/3}TiO_3$ system.[5] High Q-value ceramics were synthesized from the $(1-x)CaTiO_3$–$xCa(Al_{1/2}Ta_{1/2})O_3$ solid-solution system, which at $x \sim 0.5$ exhibited $\tau_f \sim 0$ ppm/K.[6] Special attention was paid to the suppression of $\tau_f$ in the investigation of $(1-x)ATiO_3$–$xLa(Zn_{1/2}Ti_{1/2})O_3$ ($A$ = Ca, Sr) by Cho et al.[7] They observed that in both systems $\tau_f$ decreases with the increase in $x$ in a similar manner. Highly positive values of $\tau_f$ are completely compensated with 50 mol% of $La(Zn_{1/2}Ti_{1/2})O_3$.

The highest $Q$-values among the microwave ceramics based on alkaline-earth titanates were reported for the $(1-x)SrTiO_3$–$xLaAlO_3$ ceramics.[8] The system exhibits

* Corresponding author.
*E-mail address:* bostjan.jancar@ijs.si (B. Jancar).

0955-2219/02/$ - see front matter © 2002 Elsevier Science Ltd. All rights reserved.
PII: S0955-2219(02)00359-X

solid solubility across the entire compositional range with the crystal structure changing from cubic to rhombohedral at $x=0.2$. With an increase in the concentration of $LaAlO_3$ the $Q$-value rapidly increases whereas $\tau_f$ and $\varepsilon_r$ decrease. It was shown that by manipulating the concentration of $LaAlO_3$ the $\tau_f$ can be suppressed and tuned. The ceramics based on the $0.55SrTiO_3$–$0.45LaAlO_3$ solid solution, with $\varepsilon_r=34$, $Qxf=69.000$ GHz and $\tau_f=-8$ ppm/K. exhibit technologically interesting microwave dielectric properties.

Because of their negative $\tau_f$ and high $Q$-values,[9] rare-earth aluminates with the perovskite structure are suitable candidates for combining with alkaline-earth titanates in order to synthesize new, high-$Q$, temperature-stable microwave dielectrics. Our investigations have shown that solid solutions with promising microwave dielectric properties can be synthesized from systems based on $(1-x)CaTiO_3$–$xREAlO_3$ ($RE$ = La, Nd and Sm).[10] We established that the variation of the dielectric properties with the increase in $x$ does not significantly depend on the nature of the $RE$. The highly positive $\tau_f$ of $CaTiO_3$ is completely suppressed by 30–35 mol% of $REAlO_3$. The $\varepsilon_r$ of the solid solutions with temperature-stable resonant frequencies are in the range 40–45 and the $Q$-values are between 35.000 and 45.000 GHz. Furthermore we showed that replacement of the $REAlO_3$ with $REGaO_3$ slightly improves the permittivitiy of solid solutions but adversely affects the $Q$-value. An attempt was made to further manipulate the microwave dielectric properties by partially substituting $Ca^{2+}$ with $Ba^{2+}$, $Sr^{2+}$ and $Mg^{2+}$. The introduction of $Ba^{2+}$ increased the $\tau_f$ and decreased the $Q$-value but did not affect the $\varepsilon_r$. The presence of $Mg^{2+}$ resulted in the formation of a spinel phase which lowered the $Q$-value but did not affect the $\varepsilon_r$ and the $\tau_f$ significantly. The partial substitution of $Ca^{2+}$ with $Sr^{2+}$ decreased the $Q$-value only slightly.

The ceramics based on $CaTiO_3$–$NdAlO_3$ solid solutions are the first from the $CaTiO_3$–$REAlO_3$ family to be produced commercially as microwave dielectric resonators. Preliminary measurements, however, indicated that the microwave dielectric losses depend on the processing parameters. The objective of this research was to investigate the structural and microstructural characteristics of this system in order to examine the possible reasons for such a dependence and to look into the possibility of optimizing the microwave dielectric properties.

## 2. Experimental

The samples in the $(1-x)CaTiO_3$–$xNdAlO_3$ system were prepared via the solid-state reaction method from commercial powders of $CaCO_3$ (Johnson Matthey 99.95%), $TiO_2$ (Johnson Matthey >99%), $Nd_2O_3$ (Johnson Matthey 99.99%) and $Al_2O_3$ (Johnson Matthey 99.99%). Stoichiometric amounts of the powders were homogenized for several hours in an ethanol suspension using a diagonal mixer with ytria-stabilized-zirconia balls as the homogenizing media. After the homogenization the alcohol was removed using a rotary evaporator and the resulting powder was pressed into pellets and calcined in the temperature range 1300–1500 °C with intermediate cooling, crushing and repressing until equilibrium was reached. The reaction sequence was monitored with X-ray diffraction analysis using a Philips PW 1710 X-ray powder diffractometer and Cu$K_\alpha$ radiation. After the calcination the powders were ball-milled for 1 h under ethanol with any tria-stabilized-zirconia laboratory planetary ball-mill, dried and isostatically pressed at 700 MPa. The pressed samples were sintered in an air atmosphere between 1350 and 1600 °C, the exact temperature depending on the composition. The sintering time was 10 h, the heating and cooling rates were 10 K/min, except in the case of the $0.7CaTiO_3$–$0.3NdAlO_3$ solid solution where the influence of sintering time and cooling rate on the dielectric losses was studied and therefore different sintering times (2, 10 and 30 h) and cooling rates (>10, 5 and 0.5 K/min) were used.

The microstructural analyses of the polished sintered surfaces were performed with the Jeol 840-JXA and Jeol JSM-5800 scanning electron microscopes (SEMs), equipped with Oxford Link-Isis energy-dispersive X-ray analysis systems. Samples for the transmission electron microscope (TEM) analysis, preformed with a Jeol 2000FX, were prepared by mechanical thinning and subsequent ion-beam milling using argon ions at 4 kV.

The microwave dielectric measurements were preformed with a HP 8719C network analyzer using a cavity-reflection method. The ceramic resonators with a diameter-to-height ratio of approximately 0.4 were placed in the gold-plated metal cavity with a diameter of 50 mm and a height of 30 mm. The permittivities of the ceramic resonators were calculated from the $TE_{01\delta}$ resonance frequency using the Itoh-Rudokas model[12] and the $Q$-value was determined at the same resonance from the Smith chart by analyzing the $S_{11}$ parameter, as proposed by Kajfez and Hwan.[11] In order to measure the temperature coefficient of resonant frequency we placed test cavities in the temperature-controlled chamber and the resonant frequency was measured in the temperature range between 20 and 60 °C.

## 3. Results and discussion

### 3.1. Structural characteristics of the $(1-x)CaTiO_3$–$xNdAlO_3$ system

The X-ray spectra collected from different compositions along the $(1-x)CaTiO_3$–$xNdAlO_3$ tie line shown

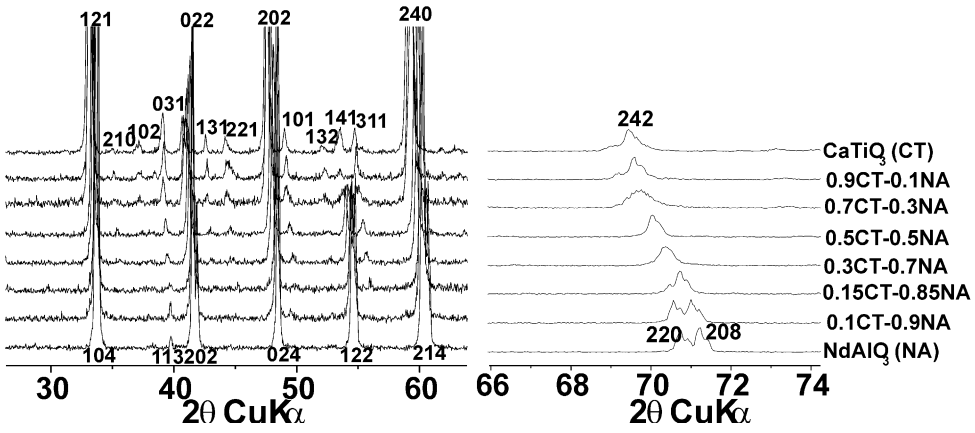


Fig. 1. X-ray diffraction patterns collected from different compositions along the $CaTiO_3$–$NdAlO_3$ tie line.

in Fig. 1 indicate complete solid solubility across the entire compositional range. Regarding the crystal structure, the X-ray analysis shows the existence of at least two distinct regions. In the range $0 < x < 0.85$ the structure of the perovskite solid solution exhibits orthorhombic symmetry similar to that of pure $CaTiO_3$ where the $[TiO_6]$ octahedra are tilted with respect to the cubic [100] and [110] directions ($a^-a^-c^+$ according to Glazers notation).[13,14] Octahedral tilting in pure $CaTiO_3$ brings about severe distortion of the $[CaO_{12}]$ polyhedron, as a result of which the $Ca^{2+}$ ion is 8 rather than 12 coordinated and the symmetry is orthorhombic (space group Pbnm). For $x > 0.90$ the solid solutions had the trigonal. This structural type is characteristic of pure $NdAlO_3$, where the $[AlO_6]$ octahedra are tilted with respect to the cubic [111] direction ($a^-a^-a^-$ according to Glazers notation) and slightly distorted, which yields the trigonal symmetry (space group R-3c).[15,16] The morphotropic phase transition occurs at a particular composition within the range between $x = 0.85$ and $x = 0.90$. Furthermore, from Fig. 2 it is clear that in the orthorhombic region the increase in $x$ causes the convergence of the unit-cell parameters, expressed in terms of a one-formula-unit pseudo cell. Since the initial differences in the length of the pseudo-cell edges ($a_p \sim 3.850$ Å, $b_p \sim 3.810$ Å, $c_p \sim 3.825$ Å) are directly related to the two types of octahedral tilts present in pure $CaTiO_3$, such behavior indicates the gradual decrease of the octahedral-tilting-induced orthorhombic distortion with the increase in the $NdAlO_3$ concentration.

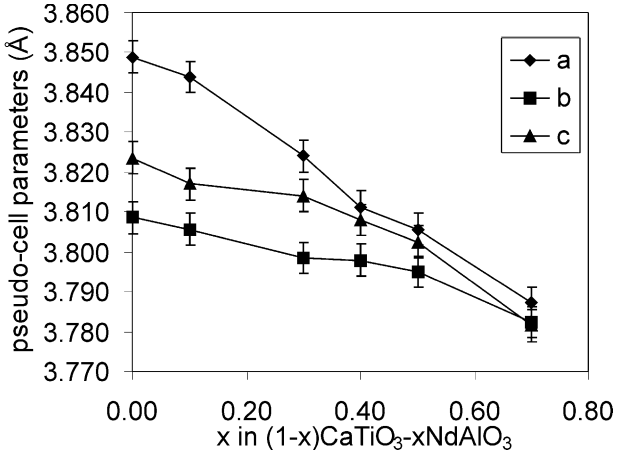


Fig. 2. Parameters of the one-formula-unit pseudo cell as a function of $x$ in $(1-x)CaTiO_3$–$xNdAlO_3$.

The nature and magnitude of the deformation of the perovskite structure is associated with the ratio between the average size of the ionic radii on the A and B sites.[17] With the increase of the tolerance factor ($t$) toward $t = 1$ the distortion of the perovskite structure changes from orthorhombic to trigonal. Consistently, for $(1-x)CaTiO_3$–$xNdAlO_3$ solid solutions the increase in $x$ results in the gradual increase of the tolerance factor from 0.966 at $x = 0$–0.976 at $x = 1$ (ionic radii according to Shannon[18]), which results in the transition from orthorhombic to trigonal distortion.

### 3.2. Microstructural characteristics

A qualitative comparison of the etched, sintered surfaces of ceramics with compositions from the $CaTiO_3$–$NdAlO_3$ tie line reveals a typically low level of residual porosity (less than 3%) and a decrease of the average grain size (from approximately 15 μm at $x = 0.15$ to approximately 5 μm at $x = 0.4$) with the increase in $x$. (Fig. 3). A more detailed microstructural investigation was preformed on a ceramic with the composition $0.7CaTiO_3$–$0.3NdAlO_3$, which according to the exhibited microwave dielectric properties is the most suitable candidate for use in wireless telecommunication devices.[19] The powder of the $0.7CaTiO_3$–$0.3NdAlO_3$ solid solution, with an average particle size of approximately 1.4 μm, sinters to a high density at 1450 °C. The time required to achieve an estimated relative density of more than 95% at this temperature is less than 2 h. Prolonged sintering times strongly influence the average grain size, which increases from approximately 8 μm

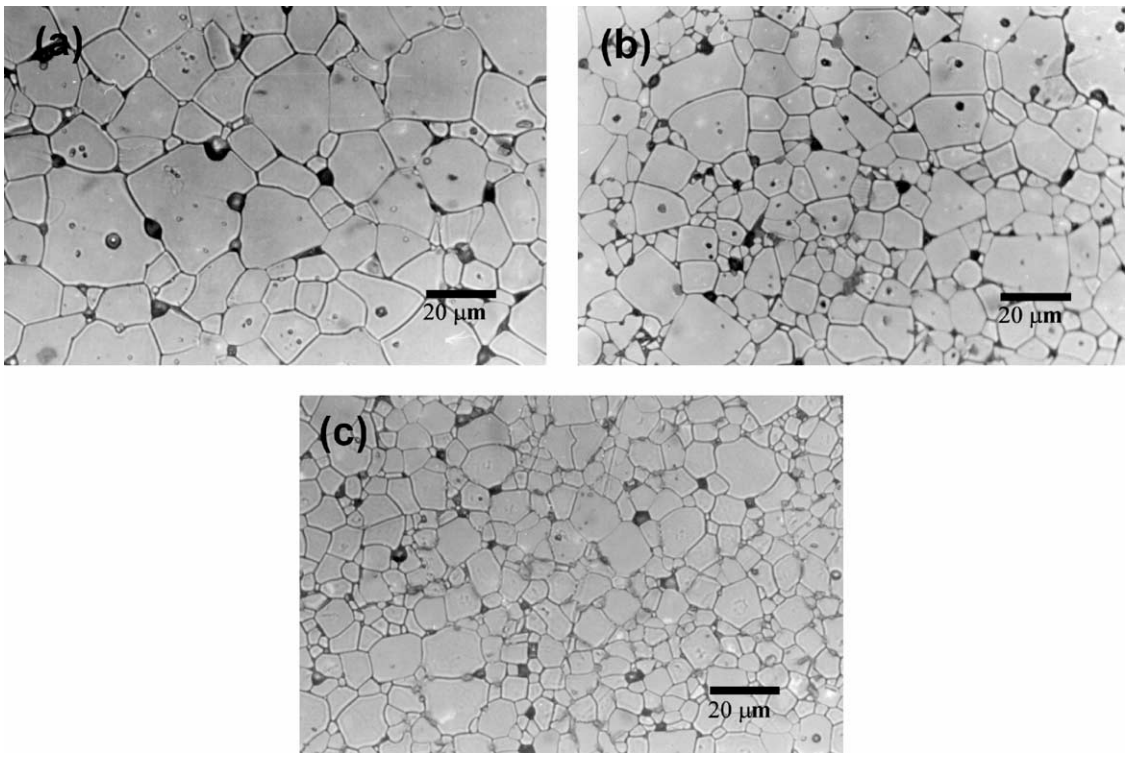


Fig.3. Microstructures of the $(1-x)CaTiO_3$–$NdAlO_3$ ceramics sintered at 1450 °C for 10 h and thermally etched at 1370 °C for 20 min. (a) $x=0.15$, (b) $x=0.3$, (c) $x=0.4$.

after 2 h to approximately 20 μm after 30 h (Fig. 4). With more efficient ball-milling the particle size of the starting powder can be lowered to an average size of 0.7 μm, which reduces the sintering temperature to 1350 °C. Lowering the sintering temperature from 1450 to 1350 °C does not significantly influence the microstructural features and microwave dielectric properties of the $0.7CaTiO_3$–$0.3NdAlO_3$ ceramics.

The TEM analysis of the sintered ceramics revealed the presence of four distinct microstructural features: twin domains, antiphase boundaries and two types of Al-rich inclusions. The presence of the domain structure within the individual grains is clearly visible in the bright-field electron micrograph shown in Fig. 5. The selected-area-electron-diffraction (SAED) patterns collected from the individual domains shown in Fig. 6 reveal the following relationships: Domain 1 can be transformed into domain 2 via a 180° rotation about the normal of the (112) plane, which is equivalent to a reflection operation across the (112) crystallographic plane. Domain 3 can be transformed into domain 1 via a 90° rotation about the normal to the (110) plane, which is equivalent to a reflection operation across the (112) plane. The overall electron-diffraction pattern collected from the three adjacent domains of Fig. 6(a), shown in Fig. 6(e), is the sum of the diffraction patterns of the individual domains. Such relationships indicate that the domains are in fact (112) reflection twins, which are also present in the natural perovskite.[20–22] The presence of these twins in perovskite crystals is a consequence of a symmetry-breaking octahedra-tilting phase transition where a space group of a lower-symmetry polymorph is a subgroup of a higher-symmetry one. [23,24]

Fig. 7 shows a bright-field electron micrograph of the antiphase boundaries (APB) in a $0.7CaTiO_3$–$0.3NdAlO_3$ ceramic. The presence of the APBs in a crystal is indicative of the structural phase transition where the daughter phase belongs to the same crystal class as the parent phase but lacks the translational symmetry.[23] Examples of such cases are cation disorder-order transitions and transitions resulting in doubling of the unit cell due to antiphase octahedral tilting. In order to determine the origin of the APBs we examined the possibility of cation ordering. Since the atomic scattering factors of Ca ($f' \sim 20$ e/atom at 8 keV) and Nd ($f' \sim 56$ e/atom at 8 keV) on the A-site as well as those of Ti ($f' \sim 22$ e/atom at 8 keV) and Al ($f' \sim 13$ e/atom at 8 keV)[25] on the B-site differ considerably, the superstructure reflections due to cation ordering should be clearly visible in the X-ray pattern. In the case of 1:1 ordering a superstructure reflection would appear at 1/2(111) of the cubic aristotype (1/2(102) of the orthorhombic hettotype), which is at approximately $2\theta = 18.5°$. The X-ray pattern of the $0.7CaTiO_3$–$0.3NdAlO_3$ ceramic sintered at 1450 °C and slow cooled with a rate of 0.5 K/min was collected with a step size of 0.02° of $2\theta$ and a 4 s per step count time, shown in Fig. 8, does not

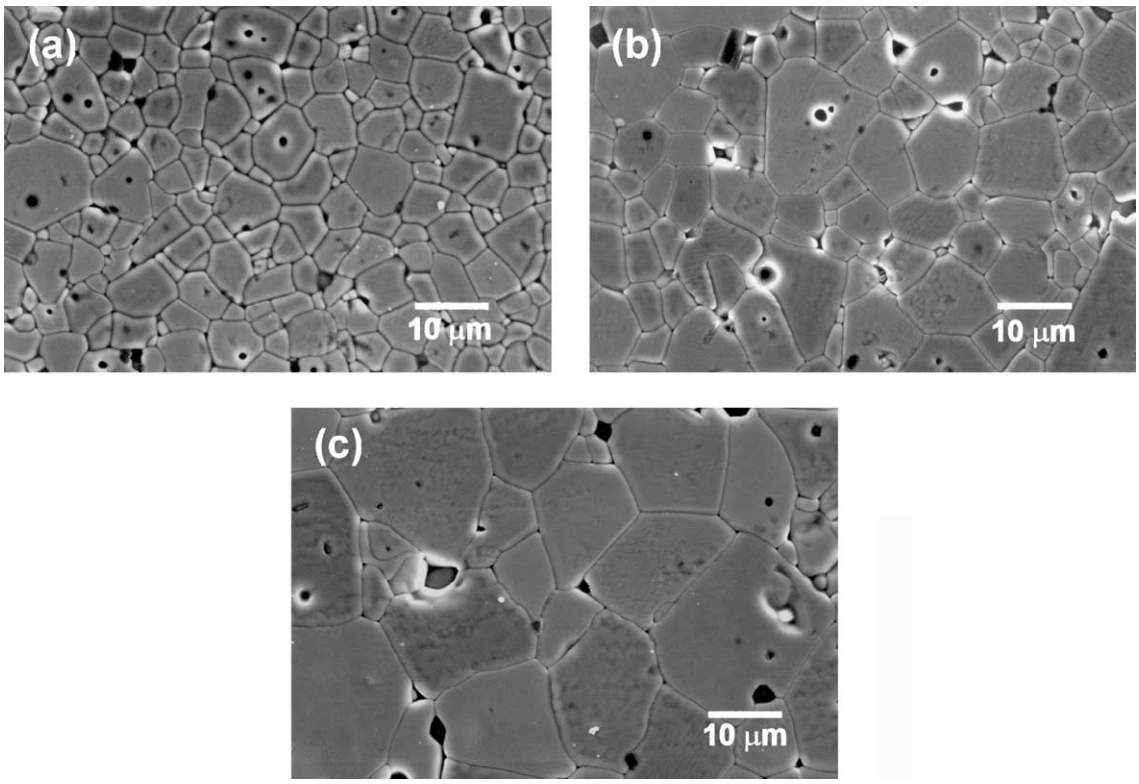


Fig. 4. Microstructures of the $0.7CaTiO_3$–$0.3NdAlO_3$ ceramics sintered at 1450 °C (a) 2 h, (b) 10 h and (c) 30 h and thermally etched at 1370 °C for 20 min.

exhibit any superstructure peaks that would indicate cation ordering. Therefore, we can conclude that the presence of APBs is not due to the disorder–order transition but rather due to a structural phase transition involving antiphase tilting of the [$BO_6$] octahedra.

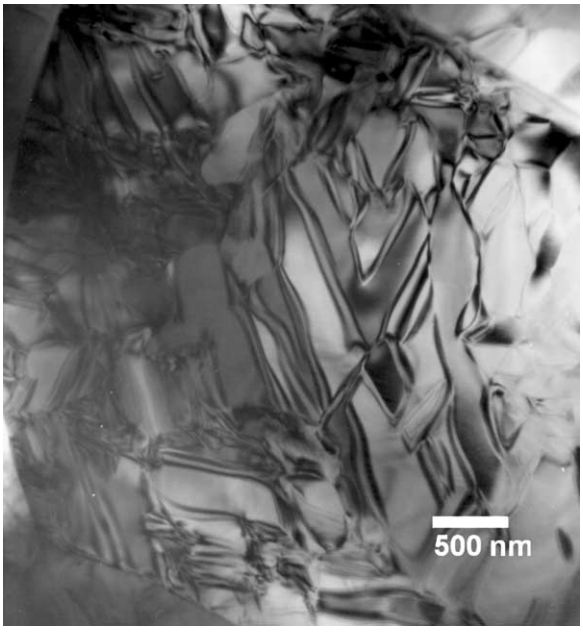


Fig 5. Bright-field TEM image of a single grain in the $0.7CaTiO_3$–$0.3NdAlO_3$ ceramics sintered at 1450 °C.

Similar microstructures containing twins and APBs were observed in natural and synthetic $CaTiO_3$. By using high-temperature X-ray and high-temperature neutron-diffraction analyses it was established that $CaTiO_3$ at temperatures above 1000 °C undergoes several structural phase transitions involving the tilting of the [$TiO_6$] octahedra.[26–28] It was also shown that with the increase in temperature the magnitudes of octahedral tilts gradually decrease until at a certain temperature the Ti–O–Ti bond angle reaches 180° and the structure becomes cubic. The presence of twins and APBs in the $0.7CaTiO_3$–$0.3NdAlO_3$ ceramic thus indicates that upon cooling from the sintering temperature these ceramics undergo octahedral-tilting phase transitions similar to those of pure $CaTiO_3$. Both microstructural features are present in the ceramics also after lowering the sintering temperature to 1350 °C, which indicates that the structural phase transitions in the $0.7CaTiO_3$–$0.3NdAlO_3$ solid solution take place below this temperature.

Domain walls, which are present in the microstructure due to the existence of the domain structure, are the source of the extrinsic dielectric losses. Since the presence of the domain structure is a direct consequence of structural phase transitions that take place upon cooling of the $0.7CaTiO_3$–$0.3NdAlO_3$ solid solution from the processing temperature, it could only be avoided by lowering the calcination and sintering temperatures

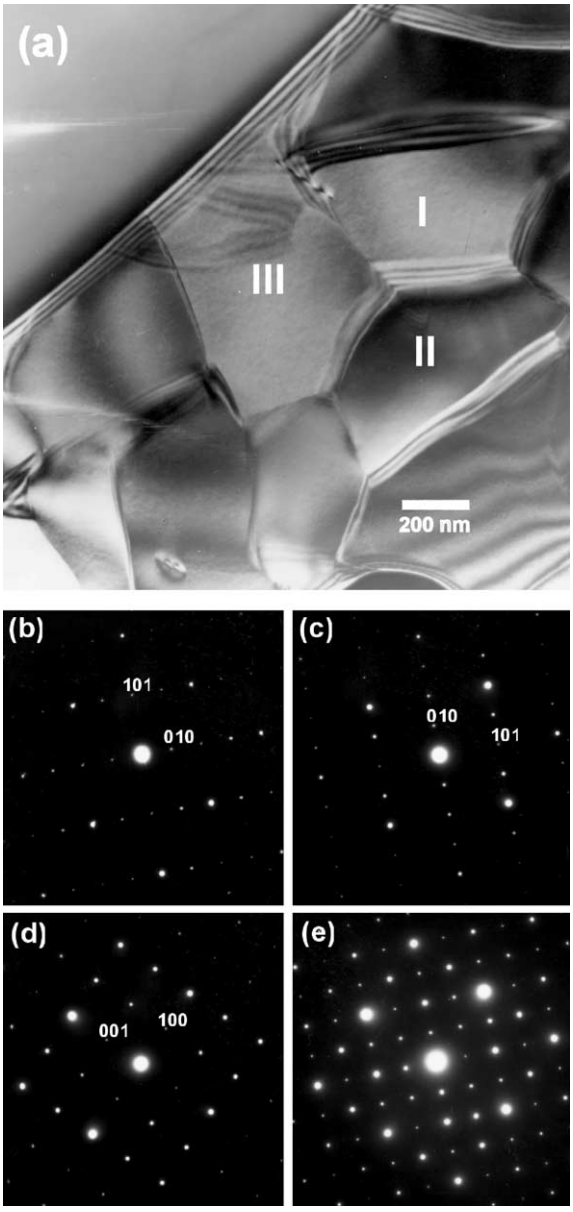


Fig 6. (a) Bright-field TEM image of the domains in $0.7CaTiO_3$–$0.3NdAlO_3$ ceramics and the selected-area electron-diffraction (SAED) patterns of (b) domain I, (c) domain II, (d) domain III and (e) the composite SAED pattern. Patterns are indexed according to the $CaTiO_3$-type orthorhombic unit cell.

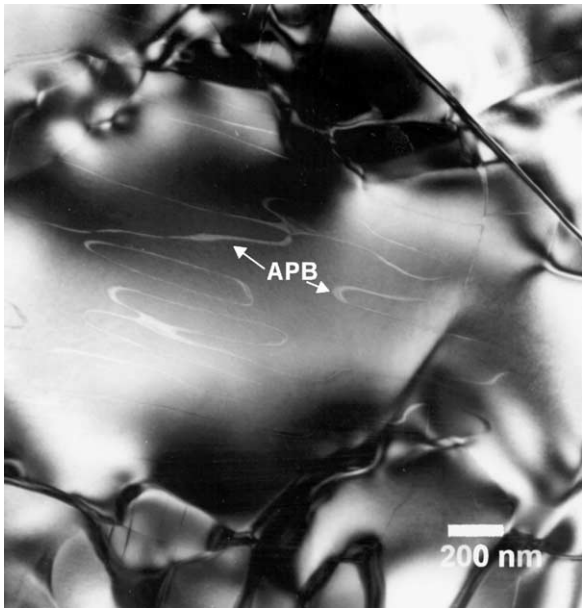


Fig. 7. Bright-field TEM micrograph of the antiphase boundaries (APBs) in $0.7CaTiO_3$–$0.3NdAlO_3$ ceramics sintered at 1450 °C.

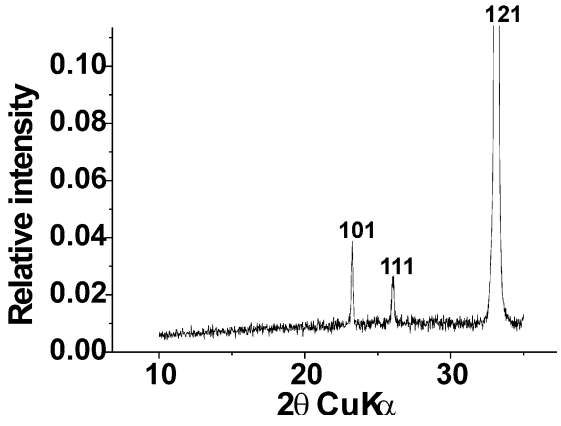


Fig 8. : Low-angle region of the X-ray pattern of the $0.7CaTiO_3$–$0.3NdAlO_3$ solid solution sintered at 1450 °C for 10 h and cooled at a rate of 0.5 K/min. In the case of cation ordering a superstructure reflection would be present at $2\theta \sim 18.5°$.

below the temperature of the structural phase transitions. In the scope of this investigation the sintering temperature of the $0.7CaTiO_3$–$0.3NdAlO_3$ solid solution could not be reduced below 1350 °C and therefore the contribution of the domain structure to the dielectric losses of the ceramics was always present.

Fig. 9 shows the presence of inclusions in the $0.7CaTiO_3$–$0.3NdAlO_3$ ceramic. These inclusions, which are always present in the microstructure of the sintered $CaTiO_3$–$NdAlO_3$ ceramic regardless of the sintering conditions, are of two different types: elongated inclusions with sizes ranging from 1 to 5 μm, and cubic inclusions with sizes up to 2 μm. The TEM/EDS analysis indicates that the elongated inclusions are rich in Al and contain small amounts of Ca and Nd. Further analysis utilizing SAED (Fig. 10) revealed that the inclusions possess a hexagonal symmetry with a large unit cell ($a \sim 5.4$ Å, $c \sim 20.8$ Å), which is a characteristic of magnetoplumbite and β-alumina-type structures. Based on these findings we can conclude that the elongated inclusions are $CaAl_{12}O_{19}$ that contain some Nd. According to TEM/EDS analysis the cubic inclusions contain Mg and Al. The SAED pattern shown in Fig. 11 reveals a cubic symmetry with the *d*-values corresponding to those of the spinel-$MgAl_2O_4$ phase. Mg is introduced into the system as an impurity and instead of incorporating into the perovskite matrix it reacts with

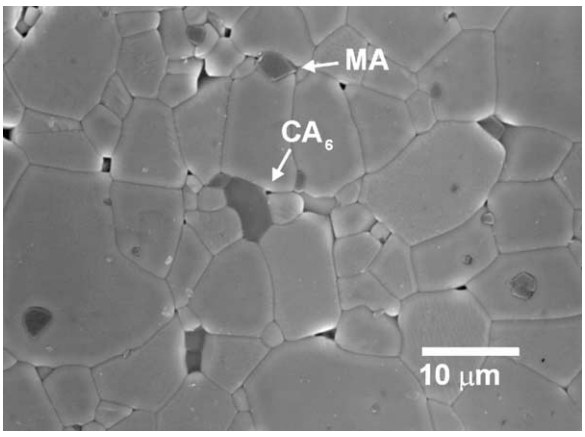


Fig. 9. Secondary-electron image of $0.7CaTiO_3$–$0.3NdAlO_3$ ceramic sintered at 1450 °C for 10 h and thermally etched at 1370 °C for 20 min. The arrows indicates the presence of a $CaAl_{12}O_{19}$-based inclusion ($CA_6$) and a spinel-$MgAl_2O_4$ inclusion (MA).

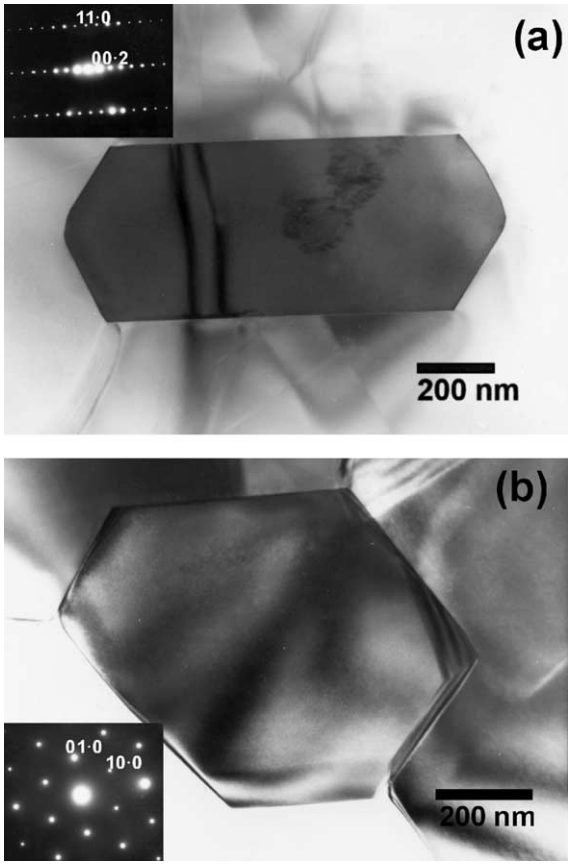


Fig 10. Bright-field TEM images of a $CaAl_{12}O_{19}$-based hexagonal inclusion and the corresponding SAED patterns (a) $z=[1\bar{1}0]$, (b) $z=[001]$.

$Al_2O_3$ to form the more stable spinel phase. The presence of these two types of Al-rich inclusions necessarily leads to the $Al^{3+}$ deficiency and thus to the local non-stoichiometry of the perovskite matrix.

The concentration of both types of Al-rich inclusions in the microstructure of the $0.7CaTiO_3$–$0.3NdAlO_3$ ceramics is relatively low (below 1%) and it does not significantly depend on the sintering conditions.

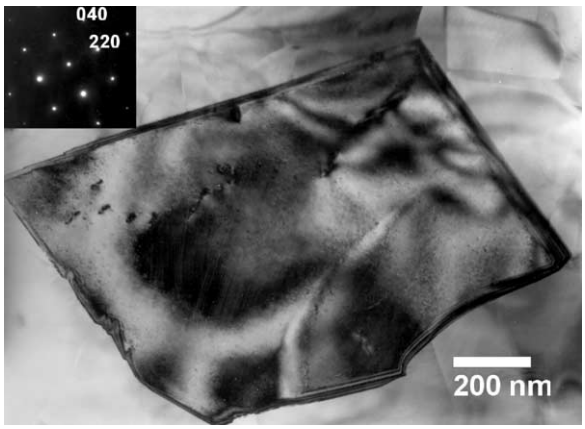


Fig 11. : Bright-field TEM image of a spinel-$MgAl_2O_4$ inclusion and an SAED pattern collected along the [001] zone axis.

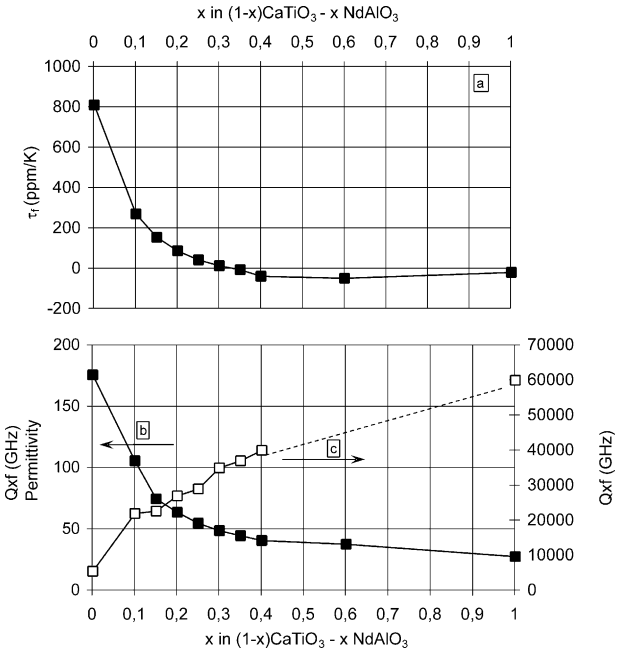


Fig. 12. Microwave dielectric properties as a function of $x$ in $(1-x)CaTiO_3$–$xNdAlO_3$ ceramics, measured at ~5 GHz (a: $\tau_f$, b: $\varepsilon_r$, c: $Q\times f$).

### 3.3. Microwave dielectric properties

With the increase in $x$ of the $(1-x)CaTiO_3$–$xNdAlO_3$ solid solution the temperature coefficient of resonant frequency and the permittivity decrease whereas the $Q$-value increases (Fig. 12).[17] These variations in dielectric properties of the sintered ceramics are not linear with x, but are significantly more pronounced for low $NdAlO_3$ concentrations. The initial increase to $x=0.1$ results in the decrease of $\tau_f$ from +800 ppm/K to +260 ppm/K whereas with the increase in $x$ from 0.3 to 0.4 the $\tau_f$ decreases from 0 to −50 ppm/K. The decrease in

permittivity with the increase in×exhibits a similar trend. The initial increase in $x$ from 0 to 0.1 reduces the $\varepsilon_r$ from 170 to 100 whereas a further increase in $x$ to 0.4 reduces $\varepsilon_r$ to 35. This indicates that the initial increase in the concentration of $NdAlO_3$ has a stronger effect on the $\tau_f$ and $\varepsilon_r$ than subsequent additions. Such behavior has also been observed in other solid-solution systems involving $CaTiO_3$ or $SrTiO_3$.[6–8] The common feature of these two perovskites is that they exhibit a polar soft mode but never undergo a ferroelectric phase transition. Such dielectrics are called quantum paraelectrics or incipient ferroelectrics. A characteristic of incipient ferroelectricity is a relatively high permittivity, a relatively large negative temperature coefficient of permittivity and consequently a highly positive temperature coefficient of resonant frequency.[29] The observed behavior of the dielectric properties of the $CaTiO_3$–$NdAlO_3$ system thus suggests that small amounts of $NdAlO_3$ effectively suppress the incipient ferroelectricity of pure $CaTiO_3$.

The highly positive $\tau_f$ of pure $CaTiO_3$ (+800 ppm/K) is completely suppressed at $x=0.3$. The permittivity of the ceramics with such a composition is 45. The peculiarity is its $Q$-value, which strongly depends on the cooling rate after sintering. Table 1 shows the $Q\times f$ values of $0.7CaTiO_3$–$0.3NdAlO_3$ ceramic sintered at 1450 °C and cooled with three different rates. As we can see from Table 1 the slower cooling rates result in ceramics with considerably higher $Q$ values. Several possibilities for such behavior were investigated. The dependence of the $Q$-value on the cooling rate is a characteristic of various complex perovskite systems that exhibit B-site cation ordering. Since the cation ordering is generally a relatively slow process, the slower cooling rate usually results in a higher degree of order, which in most cases significantly lowers the dielectric losses. In the case of the $0.7CaTiO_3$–$0.3NdAlO_3$ solid solution, however, no cation ordering was found. Another possible reason for the dependence of the $Q$-value on the cooling rate after the sintering could be a partial reduction of the $Ti^{4+}$ and the presence of oxygen vacancies.[30] Since the ions reduced at high sintering temperatures tend to reoxidize during the cooling stage, a slower cooling rate usually results in lower dielectric losses. Since this mechanism is necessarily influenced by the oxygen partial pressure during processing we preformed the sintering in an oxygen atmosphere with an oxygen partial pressure of 10 bars. The dielectric properties of these oxygen-sintered samples did not differ significantly from the properties of the samples sintered in air (Table 1). Consequently we can conclude that the reduction and subsequent reoxidation is not likely to be the reason for the dependence of the $Q$-value on the cooling rate.

A slower cooling rate results in ceramics with a higher average grain size. The influence of grain size on the dielectric losses was examined in a separate experiment. Table 2 shows the $Q$-values of $0.7CaTiO_3$–$0.3NdAlO_3$ ceramics sintered at 1450 °C for 2, 10 and 30 h, the corresponding microstructures are shown in Fig. 4. The $Q\times f$-values of the ceramics sintered for the three different times are all around 30000 GHz. These results imply that the $Q$-value of $0.7CaTiO_3$–$0.3NdAlO_3$ ceramics does not significantly depend on the grain size.

Yet another possibility for the dependence of the $Q$-value on the cooling rate after the sintering is a decomposition of the solid solution and thus the formation of secondary phases during the cooling process. In order to account for such a possibility we performed several annealing experiments. We annealed the sintered ($T_{sint}=1450$ °C/10 h) $0.7CaTiO_3$–$0.3NdAlO_3$ ceramics for 10 h at five different temperatures: 1000, 1100, 1200, 1300 and 1400 °C, after each annealing the ceramics were cooled at a rate of >10 K/min. Table 3 shows the microwave dielectric properties of the ceramics after each annealing. As can be seen from Table 3 the annealing does not significantly influence the dielectric losses of the ceramics. These results and the fact that no additional secondary phases were detected either by X-ray diffraction analysis or by SEM and TEM, imply that the decomposition of the $0.7CaTiO_3$–$0.3NdAlO_3$ solid solution at temperatures lower than the sintering

Table 1
$Q\times f$-values of the $0.7CaTiO_3$–$0.3NdAlO_3$ ceramics sintered at 1450 °C/10 h in air and at $P_{O2}=10$ bars, cooled at three different rates

| Cooling rate. (K/min) | $f_r$ (GHz) | $Q\times f$ (GHz) | |
|---|---|---|---|
| | | Air | $P_{O2}=10$ bars |
| >10 | 4.872 | 30.000 | 32.000 |
| 5 | 4.883 | 38.000 | 37.000 |
| 0.5 | 4.911 | 44.000 | 43.000 |

Table 2
$Q\times f$-values of the $0.7CaTiO_3$–$0.3NdAlO_3$ ceramics sintered in air at 1450 °C as a function of dwell time (cooled with >10 K/min)

| Sintering time (h) | $f_r$ (GHz) | $Q\times f$ (GHz) |
|---|---|---|
| 2 | 4.926 | 32.000 |
| 10 | 4.922 | 31.000 |
| 30 | 4.948 | 32.000 |

Table 3
$Q\times f$-values of the $0.7CaTiO_3$–$0.3NdAlO_3$ ceramics sintered in air at 1450 °C/10 (cooled with >10 K/min) h after annealing at different temperatures for 10 h

| Annealing temperature (°C/10 h) | $f_r$ (GHz) | $Q\times f$ (GHz) |
|---|---|---|
| 1000 | 4.893 | 31.000 |
| 1100 | 4.914 | 30.000 |
| 1200 | 4.975 | 32.000 |
| 1300 | 4.952 | 32.000 |
| 1400 | 4.933 | 32.000 |

temperature is not the reason for the dependence of the $Q$-value on the cooling rate after the sintering.

One of the reasons for the dependence of the $Q$-value on the cooling rate can be the occurrence of the symmetry-breaking, octahedra-tilting transitions. The presence of APBs for instance, which is a direct consequence of the tilting transition, can influence the energy-inherence of the lower-symmetry phase, as it was proposed by Davies et al.[31] They claimed that the presence of APBs in the perovskites increases the free energy of the structure and thus negatively influences the $Q$-value. Since the antiphase domains usually form via a nucleation-and-subsequent-growth mechanism, the amount and the morphology of their boundaries can strongly depend on the thermal history of the structure. However, in the case of $0.7CaTiO_3$–$0.3NdAlO_3$ ceramics the influence of the structural phase transitions on the $Q$-value has not been experimentally confirmed nor has the quantitative relationship between the cooling rate, structural phase transition(s), domain formation and consequent microwave dielectric losses been determined.

## 4. Conclusions

The $(1-x)CaTiO_3$–$xNdAlO_3$ perovskite system exhibits solid solubility across the entire compositional range ($0<x<1$). With an increase in the $NdAlO_3$ concentration the magnitude of the orthorhombic distortion gradually decreases and at a particular composition in the range between $x=0.85$ and $x=0.9$ a transition to the trigonal structure occurs. With the increase in $x$ the temperature coefficient of resonant frequency ($\tau_f$) and the relative permittivity ($\varepsilon_r$) decrease, whereas the $Q$-value increases. Ceramics based on the $0.7CaTiO_3$–$0.3NdAlO_3$ solid solution exhibit $\tau_f=0$ ppm/K, $\varepsilon_r=45$ and a $Q$-value that strongly depends on the cooling rate after sintering. With a cooling rate of 0.5K/min ceramics exhibit a $Q\times f=45.000$ GHz, whereas with a cooling rate higher than 10 K/min the $Q\times f$ is 30.000 GHz. An X-ray analysis of the slow-cooled ceramics did not reveal any kind of cation ordering. The microstructural investigation of such ceramics revealed the presence of twin boundaries, antiphase boundaries and two types of Al-rich inclusions: the hexagonal $CaAl_{12}O_{19}$-based inclusions and the spinel $MgAl_2O_4$, which forms as a result of the presence of Mg-based impurities.

## References


1. Kell, R. C., Greenham, A. C. and Olds, G. C. E., High-permittivity temperature-stable ceramic dielectrics with low microwave loss. *J. Am. Ceram. Soc.*, 1973, **56**(7), 352–354.
2. Moon, J. H., Jang, H. M., Park, H. S., Shin, J. Y. and Kim, H. S., Sintering behavior and microwave dielectric properties of (Ca, La)(Ti, Al)$O_3$ ceramics. *Jpn. J. Appl. Phys.*, 1999, **38**(12A), 6821–6826.
3. Kim, J. S., Cheon, C. I., Kang, H. J. and Lee, C. H., Crystal structure and microwave dielectric properties of $CaTiO_3$–$(Li_{1/2}Nd_{1/2})TiO_3$–$(Ln_{1/3}Nd_{1/3})TiO_3$ (Ln = La, Dy) ceramics. *Jpn. J. Appl. Phys.*, 1999, **38**(9B), 5633–5637.
4. Kim, I. S., Jung, W. H., Inaguma, Y., Nakamura, T. and Itoh, M., Dielectric properties of a-site deficient perovskite-type lanthanum–calcium–titanium oxide solid solution system [$(1-x)La_{2/3}TiO_3$–$xCaTiO_3$ ($0.1\leqslant x\leqslant 0.96$)]. *Mater. Res. Bull.*, 1995, **30**(3), 307–316.
5. Yoshida, M., Hara, N., Takada, T. and Seki, A., Structure and dielectric properties of $(Ca_{1-x}Nd_{2x/3})TiO_3$. *Jpn. J. Appl. Phys.*, 1997, **36**(11), 6818–6823.
6. Kucheiko, S., Choi, J. W., Kim, H. J. and Jung, H. J., Microwave dielectric properties of $CaTiO_3$–$Ca(Al_{1/2}Ta_{1/2})O_3$ ceramics. *J. Am. Ceram. Soc.*, 1996, **79**(10), 2739–2743.
7. Cho, S. Y., Youn, H. J., Lee, H. J. and Hong, K. S., Contribution of structure to temperature dependence of resonant frequency in the $(1-x)La(Zn_{1/2}Ti_{1/2})O_3$–$xATiO_3$ (A = Ca, Sr) system. *J. Am. Ceram. Soc.*, 2001, **84**(4), 753–758.
8. Sun, P. H., Nakamura, T., Shan, Y. J., Inaguma, Y., Itoh, M. and Kitamura, T., Dielectric behavior of $(1-x)LaAlO_3$–$xSrTiO_3$ solid solution system at microwave frequencies. *Jpn. J. Appl. Phys.*, 1998, **37**(10), 5625–5629.
9. Cho, S. Y., Kim, I. T. and Hong, K. S., Microwave dielectric properties of rare earth aluminates. *J. Mater. Res.*, 1999, **14**(1), 114–119.
10. Jancar, B., Suvorov, D. and Valant, M., Microwave dielectric properties and microstructural characteristics of aliovalently doped perovskite ceramics based on $CaTiO_3$. *Key. Eng. Mat.*, 2002, **206-212**, 1289–1292.
11. Kajfez, D. and Hwan, E. J., $Q$-factor Measurements with network analyser. *IEEE Trans. MTT.*, 1984, **MTT-32**(1), 666–670.
12. Itoh, T. and Rudokas, R. S., New method for computing the resonant frequencies of dielectric resonator. *IEEE Trans. MTT.*, 1977, **MTT-8**(1), 52–54.
13. Glazer, A. M., The classification of tilted octahedra in perovskites. *Acta Cryst.*, 1972, **B28**, 3384–3392.
14. Glazer, A. M., Simple ways of determining perovskite structures. *Acta Cryst.*, 1975, **A31**, 756–762.
15. Marezio, M., Dernier, P. D. and Remeika, J. P., The crystal structures of orthorhombic $SmAlO_3$ and of trigonal $NdAlO_3$. *J. Solid State Chem.*, 1972, **4**, 11–19.
16. Yoshikawa, A., Horiuchi, H., Tanaka, M., Shishido, T. and Fukuda, T., Syntheses of the $(NdxSm1-x)AlO_3$ and its strusture relation to a series of rare earth orthoaluminates $RalO_3$. *J. Solid State Chem.*, 1996, **126**, 221–226.
17. Ramadass, N., $ABO_3$-type oxides-their structure and properties—a bird's eye view. *Mater. Sci. Eng.*, 1978, **36**, 231–239.
18. Shanon, R. D., Revised effective ionic radii and systematic studies of interatomic distances in halides and chalcogenides. *Acta. Cryst.*, 1976, **A 32**, 751–766.
19. Jancar, B., Suvorov, D. and Valant, M., Microwave dielectric properties of $CaTiO_3$-$NdAlO_3$ ceramics. *J. Mater. Sci. Lett.*, 2001, **20**(1), 71–72.
20. Kay, H. F. and Bailey, P. C., Structure and properties of $CaTiO_3$. *Acta Cryst.*, 1957, **10**, 219–227.
21. Wang, Y., Guyot, F. and Liebermann, R. C., Electron microscopy study of (Mg, Fe)$SiO_3$ perovskite: evidence for structural phase transitions and implications for the lower mantle. *J. Geophys. Res.*, 1992, **97**(B9), 327–347.
22. Wang, Y. and Liebermann, R. C., Electron microscopy study of domain structure due to phase transitions in natural perovskite. *Phys. Chem. Minerals.*, 1993, **20**, 147–158.
23. Wondratschek, H., Jeitschko, W. Twin domains and antiphase domains. *Acta Cryst.*, 1976 **A32**, 664–666.

24. Boulesteix, C., A Survey of domains and domain walls generated by crystallographic phase transitions causing a change of the lattice. *Phys. Stat. Sol.*, 1984 **86**(11), 11–42.
25. Chantler, C. T., Theoretical form factor, attenuation and scattering tabulation for $Z = 1$-92 from $E = 1$-10 eV to $E = 0.4$-1.0M eV. *J. Phys. Chem. Ref. Data*, 1995, **24**, 71–643.
26. Guyot, F., Richet, P., Courtial, Ph., Gillet, Ph., High-temperature heat capacity and phase transitions of $CaTiO_3$ perovskite. *Phys. Chem. Minerals.*, 1993, **20**, 141–46.
27. Redfern, S. A. T., High-temperature structural phase transitions in perovskite ($CaTiO_3$). *J. Phys.: Condens. Matter*, 1996, **8**, 8267–8275.
28. Kennedy, B. J., Howard, C. J. and Chakoumakos, B. C., Phase transitions in perovskite at elevated temperatures—a powder neutron diffraction study. *J. Phys.: Condens. Matter*, 1999, **11**, 1479–1488.
29. Lemanov, V. V. A., Sotnikov, V., Smirnova, E. P., Weihnacht, M. and Kunze, R., Perovskite CaTiO3 as an incipient ferroelectric. *Solid State Commun.*, 1999, **110**, 611–614.
30. Templeton, A., Wang, X., Penn, S. J., Webb, S. J., Cohen, L. F. and McnAlford, N., Microwave dielectric loss of titanium oxide. *J. Am. Ceram. Soc.*, 2000, **83**(1), 95–100.
31. Davies, P. K., Tong, J. and Negas, T., Effect of ordering induced domain boundaries on low-loss $Ba(Zn_{1/3}Ta_{2/3})O_3$–$BaZrO_3$ perovskite microwave dielectrics. *J. Am. Ceram. Soc.*, 1997, **80**(7), 1727–1740.